

# 2

## fMRI Scanning Methodologies

Alexander B. Pinus and Feroze B. Mohamed

### General Overview

A pervasive and constant challenge in the field of neuroscience is to advance in the understanding of working mechanisms of the human brain and what enacts such complex functions as perception, emotions, and behavior. In areas of clinical psychology, neurophysiology, and neurosciences, it is an ultimate interest to describe neuronal functions quantitatively, as well as qualitatively, under what is considered normal conditions and various disorders, and later use that knowledge for diagnostic purposes.

To investigate these complex concepts, there are a number of techniques developed to detect and characterize neuronal activity of the human brain. In recent years, technical advances in the area of magnetic resonance (MR) research and development tremendously enhanced capabilities of magnetic resonance imaging (MRI) equipment in regard to detection and characterization of minute physiological features, and unprecedentedly widened the number of applications of this modality. Such MRI and nuclear magnetic resonance (NMR) systems with superconducting magnets operating at field strengths of 8 Tesla for human<sup>1</sup> and up to 21 Tesla for animal studies<sup>2,3</sup> have lately become available, allowing extremely fine spatial resolution and considerably improved signal-to-noise ratios (SNRs). The low-noise detection electronics coupled with ultra-fast signal collection algorithms paved the way for new sensitive imaging techniques towards imaging of highly detailed static morphological features, as well as dynamic markers of physiological events and brain functions. The latter may manifest themselves through an intertwined regional changes of such physiological parameters as blood oxygenation and cerebral metabolism, blood flow and volume, and diffusion and perfusion, all of which take place coincidentally.

In the area of the *in vivo* MRI, various achievements have led to the development of methods of functional MRI (fMRI). Functional MRI is a class of techniques that exploits susceptibility of the magnetic resonance signal to certain physiological properties associated with

neuronal activity in general and intrinsic qualities of blood in particular. The most explored and developed fMRI method—Blood Oxygenation Level Dependency (BOLD)—detects tiny changes in magnetic properties of blood caused by metabolic and vascular responses to an elicited neuronal activity.

The brain activity and, in particular, pre-synaptic firings are associated with increased energy demands and are satisfied mainly by way of an oxidative glucose consumption.<sup>4-7</sup> After an onset of a particular brain activity, a nearby feeding arteriole dilates, thus causing the blood flow in downstream capillaries to increase.<sup>8,9</sup> Although during no-stimulus (baseline) conditions, all capillaries are already perfused, brain activity increases the blood flow through the capillaries in an immediate vicinity of active neurons. Because an influx of the blood flow is larger than an increase in oxygen consumption, overall oxygen concentration in blood increases, especially on the venular side of a capillary and further down in venous vessels.<sup>10,11</sup>

Due to such an increase, the blood becomes more oxygenated, which implies that the oxygen dissolved in blood gets bound to partially or fully deoxygenated heme molecules, thus turning deoxyhemoglobin to oxyhemoglobin. In a configuration with bound oxygen, ferrous iron on the heme changes its conformation and becomes more diamagnetic (less paramagnetic) as more oxygen molecules are attached to the heme. Hence, the oxyhemoglobin is more diamagnetic than the deoxyhemoglobin, and, therefore, when placed in the magnetic field of an MR scanner, imparts a different, lesser magnetic susceptibility in regard to the surroundings. The numerical and statistical evaluations of image intensity differences caused by blood magnetic susceptibility during periods of stimulated or spuriously evoked neuronal activity and periods of absence thereof may show neuroanatomical markers of such an activity.

The described phenomenon is the basis of the blood oxygenation level-dependent (BOLD) contrast employed in the fMRI. A quality and an observational value of an MRI study designed to monitor a particular brain function or a number of brain functions involved in a specific physiological or behavioral event depend on assortment of parameters and factors prescribed in a form of MRI pulse sequences.

The imaging pulse sequence is a set of instructions given by a developer to the MR scanner's data acquisition system on how to collect the MR signal and sensitize it to a particular property of the target, which could be of a morphological, functional, or chemical origin. To this end, selectivity of an acquisition protocol usually is accomplished by temporal adjustments of appropriate manipulations with magnitude and phase of the sample's bulk magnetization during the data collection process.

Of particular importance in an MR experiment is to achieve a high SNR and the tissue, or function, or chemical contrast. Higher SNR is achieved by the way of adjusting pulse sequence parameters so that maximum amount of available MR signal returned by a target is captured. Higher contrast is achieved by the way of sensitizing the MR

signal to a specific target and, in some cases, suppressing that of the target's surroundings. For instance, in order to perform a routine clinical morphological analysis, MR signal intensities of adjacent tissues have to differ by an amount appreciative to an unaided eye. Similarly, to gain functional information, for instance in a typical BOLD experiment, the nature, structure, and timing of the pulse sequence's manipulations are optimized collect most data when the MR signal related to a studied set of functions is the strongest.

It has been shown that dynamics of the MR signal, especially its decay (relaxation) rates, is dependent on the blood oxygen content.<sup>12,13</sup> In particular, increased magnetic susceptibility caused by the deoxygenation affects  $T_2^*$  and  $T_2$  relaxation processes. Such a dependence may be taken advantage of in fMRI experiments, with pulse sequences purposefully tuned to produce  $T_2^*$  or  $T_2$  contrast. Such sequences are designed to be sensitive to tiny variations of magnetic fields (microscopic field gradients) induced by changing blood oxygen content. Depending on application objectives, the target's relaxation and MR-related properties, gradient-echo signal formation mechanisms can be used to achieve  $T_2^*$  contrast, whereas the spin-echo signal formation algorithms are employed to produce the  $T_2$ -weighted contrast.

## Spin-Echo and Gradient-Echo Imaging Methods

Conventional single-echo, spin-echo, and gradient-echo signal formation algorithms have been routinely used clinical applications for years, mainly because of their versatility to produce a number of contrasts for various targets. Spin-echo imaging pulse sequences are used in an assortment of anatomical studies to produce  $T_1$ ,  $T_2$ , and proton density (PD) weighted images; gradient-echo imaging pulse sequences are more likely to be employed in formation of  $T_2$  and  $T_2^*$  image contrasts, although they are used to render the  $T_1$  image contrast, especially in higher-field strength systems. In addition, being sensitive to motion, gradient-echo imaging is used in MR angiography (MRA), volumetric evaluation studies, and those with contrast agents.

Both imaging mechanisms are sensitive to BOLD-associated microscopic field gradients imparted by the neuronal activity. The spin-echo MR signal is susceptible to local gradients due to inflow effects and irreversible diffusion dephasing that introduce  $T_2$  weighting. These factors also affect the gradient-echo MR BOLD-coupled signal. Furthermore, the MR signal detected in experiments with gradient-echo pulse sequences reflects conventional reversible  $T_2^*$  losses due to the intravoxel field distribution.

### Spin-Echo Formation Mechanism

To generate a spin echo, at least two radio frequency (RF) pulses are required—the first is used to deflect the initial longitudinal magnetization into the transverse plane, and the second is needed to recreate the lost spin phase coherence. Consider the evolution of the transverse

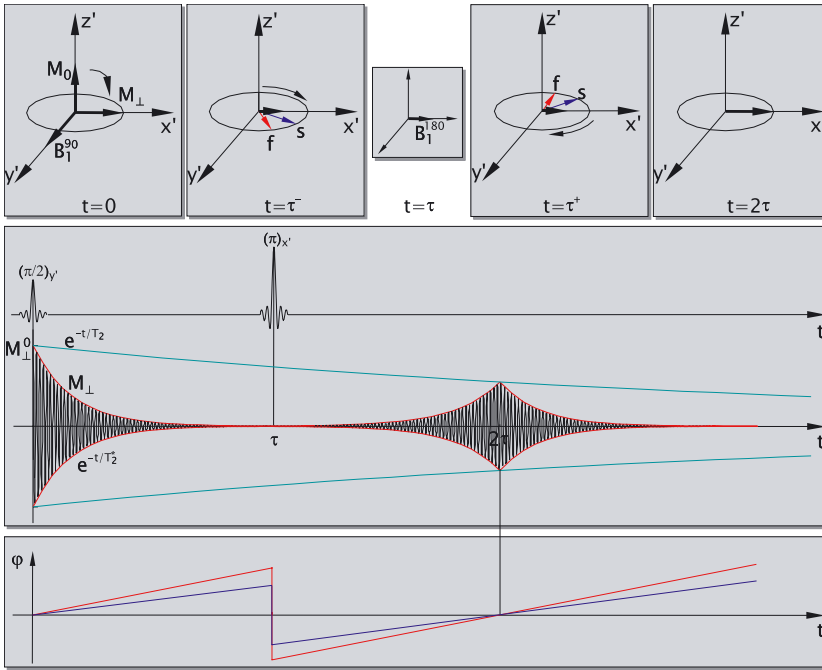


**Figure 2.1.** SE Echo: Evolution, MR Signal, Spin Phase Dynamics.

magnetization and the spin phase in the rotating reference<sup>a</sup> frame, as illustrated in the top portion of the Figure 2.1, and the process of creating the spin echo shown in the laboratory frame<sup>b</sup> in the middle part of the same figure.

At the moment of time  $t = 0$ , a  $\frac{\pi}{2}$ -radian RF pulse is applied to the sample along the  $y'$  axis, forcing the bulk magnetization into the transverse plane. As the free precession ensues, two isochromats with precessional frequencies  $\omega_f > \omega_s > \omega_0$  start to progressively lose coherence and deflect from their original direction along the  $x'$  axis. This process lasts until the free precession is somehow disrupted, for instance by another RF pulse applied at the time instance  $\tau$ . Immediately before time  $\tau$  elapses, the isochromats are separated by the phase angle  $(\omega_f - \omega_s)\tau$ ; the magnetization has diminished due to the  $T_2^*$  relaxation process.

At the moment of time  $\tau$ , an  $x'$ -axis-oriented  $\pi$ -radian pulse is applied that flips both spin isochromats over to the other half of the transverse plane. Consequently, immediately following such an operation, the vector that was ahead is now lagging behind the slower one by the same phase angle that it was leading just prior the  $\pi$ -radian RF pulse. Because the spin isochromats continue to precess in the same

<sup>a</sup> A precessing frame or reference. Spin isochromats precessing at the Larmor frequency appear stationary.

<sup>b</sup> A stationary frame of reference. All spin isochromats are seen precessing.

direction, clockwise in the graphics, and at the same rates (assuming the spin isochromats see the same field inhomogeneity throughout the echo formation), the faster isochromat starts to gain on the slower one, decreasing the deflection phase angle  $-(\omega_f - \omega_s)t$ . Because the spins get closer to each other, their coherence improves, so that the overall magnetization starts to build up. After exact same period of time  $\tau$  it took to deflect them by the aforementioned phase angle, the two isochromats become aligned again at the moment of time known as the echo time, which, in this particular scenario type of the RF echo, happens at  $T_E = 2\tau$ .

As shown in the Figure 2.1, the refocusing RF pulse is applied after the phases of individual spins have been “scrambled” and most of the transverse magnetization has vanished. However, the refocusing pulse can be applied even before the transverse magnetization fully fades away. In either case, after the refocusing RF pulse, the magnetization grows gradually and reaches its maximum amplitude. However, the MR signal magnitude at the echo is smaller than the original amplitude immediately following the first RF pulse. This is because of the phase coherence loss encountered from random field fluctuations that cannot be recovered by the refocusing RF pulse.

### Spin-Echo Imaging Pulse Sequence

The pulse sequence that implements the spin-echo measurement is shown in the Figure 2.2. In spin-echo sequences, a  $\frac{\pi}{2}$ -radian RF pulse typically is applied to excite samples' spin isochromats.

There are generally two excitation regimes, selective and non-selective, with the selectivity referring to a spatial preference of the excitation. The non-selective regime is invoked when no special arrangements are made to associate precessional frequencies of spin isochromats with their positions. Indeed, if all spin isochromats precess at the same frequency, namely the frequency given by the well-known Larmor Equation

$$\omega_0 = \gamma B_0 \quad (2.1)$$

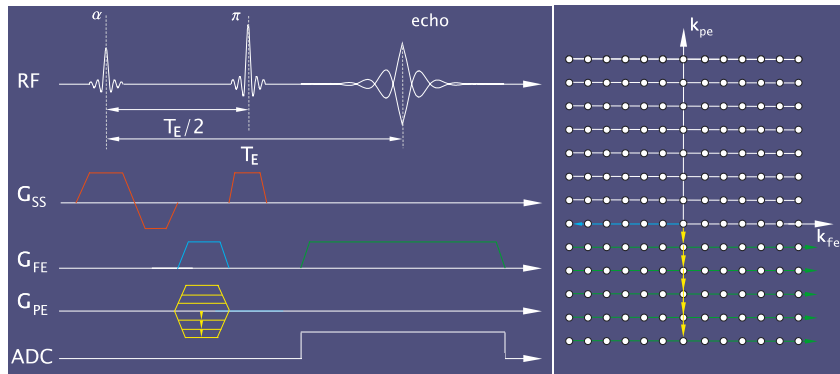
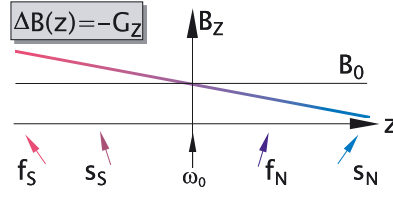


Figure 2.2. Spin Echo Timing Diagram.

Figure 2.3. The Gradient Field.



imparted by the static magnetic field  $B_0$ , it is impossible to tell isochromats apart, and therefore find their position. It also remains infeasible to establish positions of the spin isochromats if precessional rates are affected by local inhomogeneities in a random fashion, or when the inhomogeneity profile is unknown. The RF pulse that affects spins non-selectively is called hard pulse.

In order to spatially differentiate and act on a selected population of spin isochromats, precessional frequencies have to be made a function of position. It typically is achieved by an augmentation of the static magnetic field  $B_0$  with a set of supplemental magnetic fields, gradient fields, with known, and usually linear, spatial profiles. Such magnetic fields are a special kind of inhomogeneity that make spin precessional frequency position-dependent in a known fashion.

Indeed, the precessional frequency of the spin isochromat can be evaluated using a slightly modified version of the Equation (2.1), taking into consideration the gradient amplitude. For instance, if the gradient  $G_z$  is the field with an amplitude changing along  $z$  direction, the precessional frequency of spin isochromats follows the gradient profile, as shown in the Figure 2.3:

$$\omega(z) = \gamma(B_0 + B_{G_z}) = \gamma(B_0 + B_z z) = \gamma\left(B_0 + \frac{\partial B_G}{\partial z} z\right), \quad (2.2)$$

where the amplitude of the applied gradient  $G_z$  is given as the spatial partial derivative of the gradient field  $B_G$ . Similar expressions are valid for the gradients with amplitudes varying along two other axes:

$$\omega(x) = \gamma(B_0 + B_{G_x}) = \gamma(B_0 + G_x x) = \gamma\left(B_0 + \frac{\partial B_G}{\partial x} x\right), \quad (2.3)$$

$$\omega(y) = \gamma(B_0 + B_{G_y}) = \gamma(B_0 + G_y y) = \gamma\left(B_0 + \frac{\partial B_G}{\partial y} y\right). \quad (2.4)$$

The physical magnetic fields  $B_{G_x}$ ,  $B_{G_y}$ , and  $B_{G_z}$  are created by gradient coils, which are current-carrying conductors housed in the MRI system. Because the amplitudes of these fields vary in orthogonal directions, the gradient fields are said to be orthogonal.

When the linear gradient magnetic field

$$B_G = G_x x + G_y y + G_z z \quad (2.5)$$

is added to the static magnetic field  $B_0$ , precessional frequencies of spin isochromats become varied in all three directions. For a simple case of

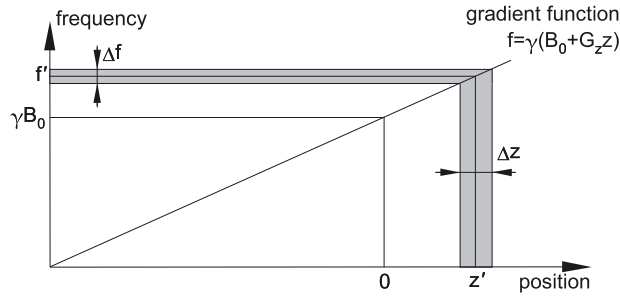


Figure 2.4. Position-Frequency Translation.

$$B_G = G_z z = G_{ss} z,$$

the association between the precessional frequency and position of a spin isochromat, as well as the translation of the RF pulse's bandwidth into the slice thickness, is shown in the Figure 2.4. The position of the slice's center  $z'$  and its thickness  $\Delta z$  can be chosen by varying the central frequency  $f'$  and either the gradient's strength  $G_z$  (the slope of the line in the graphics) or the bandwidth  $\Delta f$  of the RF pulse, respectively. Ultimately, the effect of the gradients on spin isochromats is the separation of their precessional frequencies.

If the RF pulse with a finite bandwidth, and thus a spectrum of frequencies, is applied to a population of spin isochromats frequency-separated by acting gradients fields, only those that are exposed to the pulse and precess at frequencies found within the RF pulse's bandwidth get excited. Such an excitation regime is called selective excitation, and the excitation RF pulse is called a soft pulse.

The arrangement of physical gradients, itself a vector, applied concurrently with RF pulses establishes a direction of the logical gradient called the slice selection gradient,  $G_{ss}$ . The precessional frequency of spin isochromats follows the shape of the gradient's profile, linearly varying along the gradient's direction.

Because the slice selection gradient makes precessional frequency position-dependent only in the direction of itself, the precessional frequency in two other orthogonal directions is not affected.<sup>c</sup> Therefore, the localization of spin isochromats within the slice remains unfeasible. To that end, the same principle of the position dependency can be applied to localize in-plane spin isochromats.<sup>d</sup>

As the slice selection gradient  $G_{ss}$  modulates the precessional frequency of spin isochromats, two similar gradients, frequency encoding ( $G_{fe}$ ) and phase encoding ( $G_{pe}$ ) gradients, are applied to condition spin precessional frequencies in two directions orthogonal to that estab-

<sup>c</sup> An approximation for low gradients, because Maxwell equations demand concomitant fields in orthogonal directions.

<sup>d</sup> That is spin isochromats that lie within the defined slice.

lished by the slice selection gradient. The combination of these gradients defines the spin precessional frequency in the three-dimensional (3D) space. Because each of the gradients defines its own thickness, the trio thus establishes imaging unit volumes—voxels.

The MR signal sample produced by spin isochromats in a particular voxel can be encoded in terms of frequencies varied by the gradient fields. Every such acquired sample of the MR signal comes from spin isochromats precessing at frequencies established by the arrangement of the applied gradients. The entire series of received MR signal samples for all prescribed gradient arrangement, and thus for all necessary precessional frequencies, can be placed conveniently in a matrix. The size of such a matrix and the order in which it gets filled with MR signal samples usually is determined by spatial frequency indices.

Indeed, the precessional frequency of spin isochromats in every voxel within the prescribed slice is defined by an arrangement of in-plane  $G_{fe}$  and  $G_{pe}$  gradients. Taking into consideration that the gradient field may be a function of time, the indices corresponding to the gradients usually are expressed as integrals of gradient amplitudes over their duration times:

$$k_{ss} = \gamma \int G_{ss} dt, \quad (2.6)$$

$$k_{fe} = \gamma \int G_{fe} dt, \quad (2.7)$$

$$k_{pe} = \gamma \int G_{pe} dt, \quad (2.8)$$

The received MR signal samples are therefore arranged in a form of a matrix,  $M(k_{ss}, k_{fe}, k_{pe})$ . The location of each spin isochromat is frequency-encoded in such a matrix in terms of spatial frequency  $k$  indices, and thus the received MR signal is represented in the spatial frequency space called the  $k$ -space. The depiction of the MR signal samples that make up the matrix  $M(k_{ss}, k_{fe}, k_{pe})$ , also known as  $k$ -space diagram, is shown on the right of the Figure 2.2, where the MR signal samples are represented by solid circles.

A conversion from the frequency-encoded representation of the MR signal, known as the raw MR signal, to its spatially encoded format is performed by a 3D Fourier transformation:

$$m(\mathbf{r}) = \frac{1}{2\pi} \int \int \int_{k_{ss} k_{fe} k_{pe}} M(k_{ss}, k_{fe}, k_{pe}) e^{j(\mathbf{k} \cdot \mathbf{r})} d\mathbf{r}, \quad (2.9)$$

where  $\mathbf{r}$  is the basis of the 3D spatial coordinate system. Such a process is known as image reconstruction. This equation implies that the principle prerequisite to the image reconstruction process is the availability of the raw signal matrix,  $M(k_{ss}, k_{fe}, k_{pe})$ .

After a particular MR signal sample is acquired and recorded into the current element of the raw signal matrix, one or more  $k$ -indices is incremented and the next MR signal sample is acquired and stored in the successive element of matrix. As the  $k$ -indices are advanced by



changing the amplitudes and timing of the gradients, the current element of the matrix propagates through the  $k$ -space. This process continues until the entire  $k$ -space matrix is filled<sup>e</sup> with the MR signal samples. The process of MR signal acquisition and construction of the raw signal matrix often is called the  $k$ -space coverage.

The  $k$ -space can be covered in a variety of ways. The most typical coverage path utilized in the majority of conventional pulse sequences is the sequential line-by-line traversal. Its name originates from the appearance of the  $k$ -space coverage pattern in which the order of placement of the MR signal samples in the  $k$ -space diagram gives an appearance of the line, as shown by the green arrow on the right of the Figure 2.2.

In order to implement this type of the coverage, one of the in-plane gradients is turned on for a period of time and with the amplitude needed to get the value of the corresponding  $k_{pe}$  index advanced to the location of the necessary  $k$ -space line. Such a move is shown by yellow gradient lobes on the pulse sequence graphics and corresponding arrows in the  $k$ -space diagram. At the same time, another in-plane gradient, the frequency encoding, is applied to move the index  $k_{fe}$  along just-selected  $k$ -space line to the location of the matrix element that corresponds to a first-to-be-acquired MR signal sample. This advancement is shown by the light blue color. In order to conserve imaging time, these two gradients, respectively called  $y$ - and  $x$ -offset gradient pulses, are applied simultaneously and immediately after the slice-selective excitation. The amplitude and duration of these gradients are chosen so that they conclude forwarding corresponding indices to an assigned position in the raw signal matrix before the refocusing  $\pi$ -radian RF pulse is issued, which comes at the moment  $t = \tau = \frac{T_e}{2}$  after the initial  $\frac{\pi}{2}$ -radian excitation RF pulse.

As described in the previous section, the  $\pi$ -radian RF pulse is applied to rephase spins, which were so far dephasing in the transverse plane after the initial excitation pulse. Worth noting again, the effect of such a pulse is the changed character of the precession: faster moving spins now chase slower ones, closing the gap between them. Such a motion causes spins to refocus, hence the refocusing pulse, and regain their in-plane coherence with each other, forming the MR signal echo. The MR signal echo fully develops at  $t = 2\tau = T_e$  as indicated in the Figure 2.1. The MR signal acquisition period usually starts immediately after the refocusing pulse, so that the echo would occur in the middle of it. Such an arrangement assures the most efficient imaging conditions with given imaging parameters.

During the signal acquisition period, the detection circuitry and the analog-to-digital converter<sup>f</sup> are turned on to receive and digitize the RF signal from the precessing spin isochromats. Simultaneously, the frequency encoding gradient is turned on in order to encode the preces-

<sup>e</sup> Some pulse sequences fill only a half of the  $k$ -space, which is then used to compute the other half using a property of the Hermitian complex conjugateness.

<sup>f</sup> Hence the ADC label in the Figure 2.2, and Figure 2.5.

sional frequencies with position. As long as this gradient is applied, the resonance frequency of the spin isochromats is adjusted depending on the gradient's amplitude and moment of time during which a particular sample is acquired. The signal is sampled with the prescribed sampling rate and recorded into the element of the raw MR signal matrix according to the  $k$ -space indices.

Because the signal sampling takes finite time, the effect of the longitudinal and transverse relaxations on the MR signal has to be taken in to account. That is to say, if the transverse component of the MR signal deteriorates before all samples necessary to reconstruct an image adequately are acquired, the coverage of the  $k$ -space is performed in several iterations, segments.<sup>g</sup>

In a typical and the most simple  $k$ -space coverage, such every segment corresponds to a single line. The MR signal acquisition is completed along such a line in a single repetition period,  $T_R$ . In this case, only one of the  $k$ -space indices, for instance  $k_{fe}$ , is incremented, whereas the other in-plane index,  $k_{pe}$ , is kept constant. When all necessary MR signal samples along the line are acquired, the process moves onto the next iteration, beginning with the next excitation RF pulse. This time, the amplitude of the phase-encoding gradient is incremented between the excitation and refocusing RF pulses so that the corresponding index  $k_{pe}$  is advanced to the next  $k$ -space line. Further on, the detection circuitry is turned on in the presence of the frequency-encoding gradient, and the MR signal is sampled along that  $k$ -space line.

In the description of the spin-echo formation mechanism and the corresponding pulse sequence, it was presumed that the center of the acquisition window coincides with the center of the  $k$ -space line. The center of the  $k$ -space line corresponds to an MR signal sample that has only been encoded partially with spatial information, as one of indices, namely  $k_{fe}$ , is zero.<sup>h</sup> The center of the acquisition window is taken as a point of time when the phase dispersion created by the offset gradient is compensated fully by the rephasing lobe of the read-out gradient. Only in this case does it become possible to fully eliminate the phase dispersion accrued due to fixed local field inhomogeneities.

Indeed, if the first half of the read-out gradient lasts exactly as long as the  $x$ -offset gradient and has the same amplitude, the phase of spin isochromats imparted by the gradients is zero in the center of the acquisition window. On the other hand, the phase dispersion developed due to fixed local field inhomogeneities between the excitation and refocusing pulses is nullified by the rephasing following the pulse to form what was described as the spin-echo. Therefore, when the echo time coincides with the center of the  $k$ -space line, with all other sources of the phase aberrations compensated, the overall phase disturbance is imposed only by irreversible random fluctuations due to the  $T_2$  relaxation, which are solely responsible for overall image ontrast.

<sup>g</sup> In ultra-fast imaging sequences, like echo planar imaging (EPI), the entire  $k$ -space coverage may be accomplished in a single  $T_R$  period.

<sup>h</sup> The center of the  $k$ -space lacks any spatial information, as both indices,  $k_{fe}$  and  $k_{pe}$ , are zero.

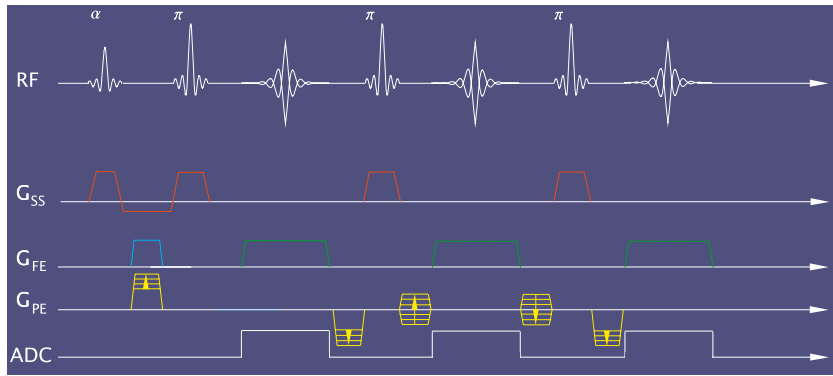


**Figure 2.5.** Fast Spin-Echo Timing Diagram.

However, it is not required for the echo time to match the moment when the  $k$ -space line's center MR signal sample is acquired along the acquisition window. The spin-echo can be arranged to occur slightly before or after that particular sample by respectively moving the refocusing pulse toward or away the excitation pulse. The spin-echo is then also moved with it, as it invariably trails the refocusing pulse by exactly the same time as the latter follows the excitation pulse. Therefore, for the spin-echo to occur by a time  $\tau$  earlier relative to the center of the  $k$ -space line, the refocusing pulse has to be transmitted by a time  $\frac{\tau}{2}$  earlier than that in the typical symmetrical arrangement. Such an offset spin-echo is referred to as the asymmetric spin-echo (ASE).

No longer in an ASE pulse sequence is the phase dispersion developed out of local inhomogeneities balanced at the moment of passing the  $k$ -space line's center, thus leaving the MR signal slightly dephased at that time. Because it is the very MR signal sample located in the center of the  $k$ -space line that contributes the most to the overall image contrast, the magnetic susceptibility effects will be reflected in the final image. Therefore, besides a general  $T_2$  contrast, an additional  $T_2^*$  weighting is introduced into the MR signal, thus making the ASE pulse sequence more sensitive to the BOLD effect.

It is possible, regardless of the echo position along the acquisition window, to cover several lines in a single iteration. The corresponding pulse sequence diagram is shown in the Figure 2.5.<sup>i</sup> Although there are multiple variations of the multi-echo acquisition scheme, such an arrangement generally is referred to as the fast spin-echo pulse sequence.

In case of such a sequence, a train of echoes is generated after a single excitation pulse by having a manifold of refocusing pulses applied to redirect spin dynamics multiple times. During every formed echo, because the MR signal is sampled along a different line, a distinct phase encoding gradient is needed. The first echo is generated in the same way

<sup>i</sup> The  $T_R$  has to be adequately short and sampling rate high to allow sufficient amount of the decaying MR signal be detected during the entire acquisition period.

a single spin-echo is formed. However, at the end of the acquisition period, a rewinder gradient is applied in the phase-encoding direction that cancels the effect of the preceding phase-encoding gradient. Such a manipulation is tantamount to a resetting of the  $k_{pe}$  index back to zero. Following the first echo, spin isochromats are allowed to continue to dephase. At some point into the dephasing process, another  $\pi$ -radian pulse is transmitted. The effect of this pulse on spins is exactly the same as that of the original refocusing pulse, namely, it swaps around faster and slower precessing spins. Immediately after the refocusing pulse, another phase-encoding gradient is applied. However, this time its amplitude is set to advance the  $k_{pe}$  to a different  $k$ -space line. The number of formed echoes, and thus the number of covered  $k$ -space lines, is given as the imaging parameter called echo train length (ETL). A number of echoes can be generated following a single RF excitation pulse, and the total acquisition time is reduced as many times as large as the ETL is.

When the entire raw signal matrix is completed for the selected slice, the process is started anew, either to acquire and average more signal for the same slice or to proceed onto another slice.

## Contrast Characteristics of Spin-Echo Sequences

### *Vascular Effects*

It was briefly mentioned that although the  $\pi$ -radian pulse refocuses acquired phase offsets by dephasing spin isochromats due to existing inhomogeneities, the phase coherence at the echo time is never restored to the pre-excitation level. Indeed, only in case of a particular spin isochromat seeing a fixed inhomogeneity throughout the acquisition can a phase angle acquired by this spin isochromat before the refocusing pulse be fully balanced out by the phase displacement that the spin isochromat experiences after the refocusing pulse. In other words, in order to fully restore spin coherence, the precessional frequency of a particular spin isochromat has to remain the same throughout the repetition period.

In reality, however, the precessional frequency of spin isochromats constantly experiences tiny aberrations that are largely imparted by the process of diffusion. A diffusing water molecule drifts in a random fashion through inhomogeneity gradients established by various physical factors, including the magnetic susceptibility caused by the BOLD effect. The degree to which the diffusion influences the spin-echo MR signal depends on the spatial range of inhomogeneities in regard to the motion extent a water molecule travels during the acquisition. If inhomogeneities vary significantly only over far larger distances than a wandering water molecule can possibly travel, then it is likely that the spin isochromats experience the same field before and following the refocusing pulse. In this case, the spin-echo is fully refocused and the MR signal does not carry the imprint of inhomogeneities. Conversely, a moving water molecule does change fields if the range of distances it travels is larger than the spatial scale of inhomogeneities. Because water molecules diffuse rather quickly, it is likely that the phase dispersion developed by molecules between two pulses is not refocused

by the time of the echo, thus leaving some dephasing to last through the echo and to attenuate the MR signal.

This line of thinking can be used in determining how the vessel size impacts the spin-echo MR signal: Because the spatial extent of inhomogeneities originated from the larger structures such as venules and arteriola spans further than that of capillaries, the diffusion-related reduction of the MR signal in capillary-rich areas is stronger than in vicinities of larger vessels. Such an argument can be substantiated by assessing the average diffusion-induced displacement a water molecule sustains and comparing it with the average vessel's size.

The average displacement  $\langle L \rangle$  over time  $t$  of a randomly moving particle can be estimated from the Einstein's diffusion equation:

$$\langle L^2 \rangle = 6\mu kTt = 6Dt, \quad (2.10)$$

where  $k \approx 1.38 \cdot 10^{-23} \left[ \frac{m^2 kg}{s^2 K} \right]$  – Boltzmann's constant;  $T$  is the temperature in Kelvins; the quantity  $D = \mu kT$  is called the diffusion coefficient, and  $\mu$  is the mobility coefficient that can be expressed through the average time between collisions  $\tau_c$  and molecular mass  $m$ :

$$\mu = \frac{\tau_c}{m}. \quad (2.11)$$

Every particle experiences about  $10^{14}$  collisions per second on average, which means that it spends  $10^{-14}$  seconds between collisions.<sup>14(p41–48)</sup> The mass of a water molecule is  $3 \cdot 10^{-26}$  kilograms. With these values, the diffusion coefficient is on the order of  $D \approx 10^{-9} \left[ \frac{m^2}{s} \right]$ . It is now possible to estimate the average displacement. Because only the in-plane displacement alters relaxation rates, the corrected expression for the average displacement is now

$$\langle L^2 \rangle = 4Dt. \quad (2.12)$$

Taking  $t = 100$  milliseconds, a typical echo time in case of the spin-echo pulse sequence, the average displacement is estimated at 20 micrometers.

It is therefore expected that the effect of diffusion in areas of venules larger than 20 micrometers in diameter gradually diminishes reversely proportional to the venule's size. This is due to the fact that the spin-echo is refocused relatively better because the water molecule spends more time in the same field. Consequently, the MR signal is changed ever so slightly. In the areas of smaller venules and larger capillaries, their diameter being on the order of 10 to 20 micrometers, the water molecule experiences different fields as it wanders in a near vicinity of vessels; hence, the spin-echo is poorly refocused and the MR signal is relatively weaker. For even smaller vessels, mostly capillaries with the lumen's diameter below 10 micrometers, the phase dispersion at the moment of spin-echo is even stronger as water molecules transgress even a larger number of fields. Therefore, it is tempting to expect relaxation rates to increase and the MR signal to lessen further. However, in

this case, the average phase dispersion encountered by all water molecules is very similar, as it is more likely that they cross over the same fields. A similar phase dispersion is tantamount to a very little phase dispersion. Therefore, counterintuitively, the spin-echo MR signal coming from areas of very small vessels, namely less than five micrometers in diameter, is in fact comparable to that acquired near the largest vessels.

Thus, the spin-echo MR signal is strongest in areas of very small and very large vessels and dips to its minimum around vessels that measure about 20 micrometers in diameter. Due to such a bell-shaped dependence of the spin-echo MR signal on the vessel's size, the spin-echo sequences are desirable to use in BOLD experiments, as the spin-echo MR signal is sensitized to the BOLD-related oxy/deoxygenated exchanges that occur in capillaries.

### *Flow Effects*

The contrast produced by the spin-echo sequences is sensitive to inflow effects and becomes apparent on  $T_2$ -weighted images. Implications of the inflow effects on the MR signal are caused primarily by spin isochromats that were brought into the region of the excited imaging volume by the blood flow following the  $\frac{\pi}{2}$ -radian excitation RF pulse.

It has been discussed earlier that only spin isochromats that initially get excited by the RF excitation pulse can return RF photons and thus contribute to the overall MR signal. Moreover, because the transverse component of the bulk magnetization is solely responsible for production of the MR signal, it is desirable to have initial large longitudinal components of as many spins as possible be transferred to the transverse plane by the excitation RF pulse in order to increase MR signal generation capacity. Finally, the refocusing RF pulse acts to minimize relative phase differences between transverse components of precessing spins and to restore the spin coherence in the transverse plane, thus yielding larger bulk magnetization and a stronger MR signal.

Consider fresh, undisturbed spins moving into already excited imaging volume. Because these spins enter between the excitation and refocusing RF pulses, they are exposed only to the  $\pi$ -radian RF pulse, which is, in effect, an excitation pulse for them, whereas it acts as a refocusing pulse for already excited spins. Unlike the latter, the freshly entered spins are forced into the excited state by the  $\pi$ -radian RF pulse. As the name of the pulse assumes, a bulk magnetization built out of these spins is rotated by 180 degrees, all the way from being oriented colinearly with the  $B_0$  to the opposite direction, thus remaining in the longitudinal plane. Therefore, such a magnetization ends up having a very small transverse component so its contribution to the MR signal generation capacity is greatly reduced. The spins that make up the 180-degree deflected magnetization eventually will return to the unexcited state, contributing little to nothing to the overall MR signal.

In the meantime, a portion of those spins within the blood that were excited along with all other stationary spins were forced to leave the imaging volume by the fresh incoming blood. The spins forced out from the imaging volume before the refocusing pulse was applied to



the same imaging volume contribute a negligible amount of the MR signal during the acquisition period because they remained dephased and did not undergo the refocusing. Those excited spins that did experience the refocusing pulse before exiting the imaging volume during the acquisition period do contribute to the MR signal. However, because their space-frequency association is now broken by the blood flow motion, they generate the MR signal that is originated from outside of the selected imaging volume, and therefore can now be regarded as flow artifacts.

The actual number of spins leaving and entering the imaging volume depends on timing characteristics of the sequence, size and position of the excited volume, and the parameters of the flow. If the time between the excitation and refocusing pulses is relatively shorter, a smaller number of excited spins is replaced by fresh ones; therefore, the MR signal would be suppressed to a lesser degree.

From another perspective, the time between the two pulses is equal to  $\frac{T_1}{2}$ . Therefore, it is optimal to keep the echo time short enough to reduce the inflow suppression, but long enough to collect sufficient amount of the MR signal with BOLD contrast. It was shown that such an optimal echo time is on the order of the  $T_2$  relaxation time of the examined tissue.<sup>15</sup>

Because the echo time is usually much shorter than the repetition time for the spin-echo sequences, the inflow suppression would become significant only for relatively high flow velocities, which typically do not occur in the capillaries and small venules, the primary source of the BOLD contrast.

### Gradient-Echo Formation Mechanism

As has already been shown, the refocusing RF pulse is essential for the spin-echo formation, as it rephases spin isochromats and leads to reappearance of the transverse magnetization. However, the rephasing action and refocusing effect of the RF pulse also can be achieved if gradient fields are employed to modulate spin phase in a controlled fashion. The MR signal is then recovered in the form of a gradient-echo generated only through gradient reversals.

Consider the gradient-echo formation mechanism in an example with a system of four spin isochromats at different locations along the  $z$  axis, so that  $z_{fs} = -z_{fN}$  and  $z_{ss} = -z_{sN}$ <sup>j</sup>, as shown in the Figure 2.3. The application of the gradient field makes spins in the North half precess slower than those in the South half. Indeed, because of the additional gradient field, the two South spins experience higher than  $B_0$  field, and they precess slightly faster in regard to the spin unaffected by the gradient field, thus precessing at the angular rate of  $\omega_0$ . Of these two South spins, the one closer to the center of the field,  $s_s$ , precesses at slower rate because the field deviation at the location of this spin is less and its precessing frequency is closer to the  $\omega_0$ . Similarly, for the North

---

<sup>j</sup> The subscripts  $f$  and  $s$  stand for fast and slow. The subsubscripts  $s$  and  $N$  stand for South and North.

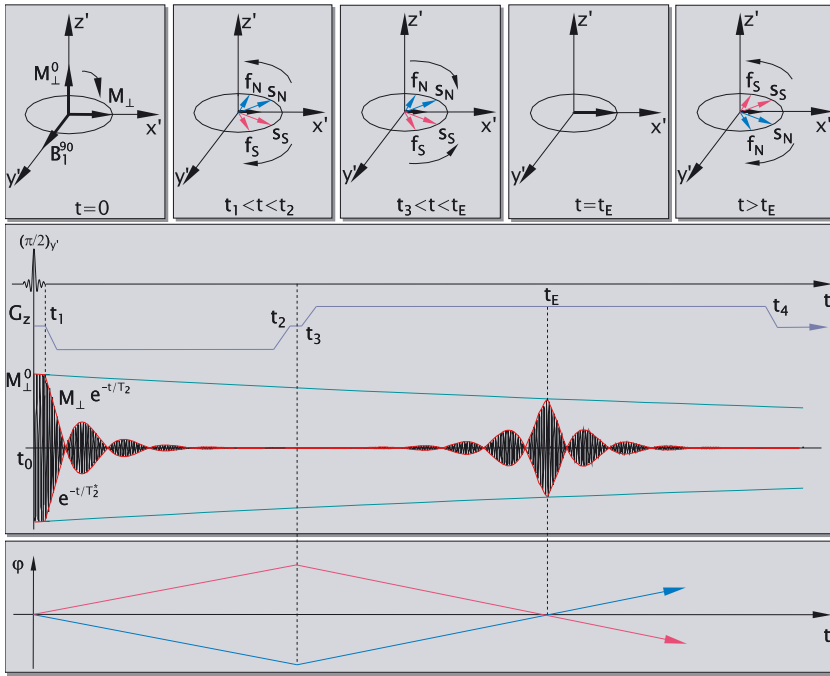


**Figure 2.6.** Gradient-Echo: Evolution, MR Signal, Spin Phase Dynamics.

section where the magnetic field is less than  $B_0$ , the spins precess generally slower than in the South section, with the one further from the center of the field,  $s_N$ , precessing slower than the  $f_N$  spin.

Therefore, the main effect of the applied gradient field is an introduced spatially dependent precessional frequency that makes spin isochromats precess at rates controlled by the amplitude of the applied gradient field. With such a dependence on the gradient field, the generation of the gradient echo can be explained phenomenologically and graphically, as is illustrated in the top of the Figure 2.6.

An excitation  $\frac{\pi}{2}$ -radian RF pulse<sup>k</sup> is applied at the moment of time  $t = 0$ , putting the longitudinal magnetization into the transverse plane. Immediately at the end of the excitation pulse, all spin isochromats precess at the same rate. However, naturally occurring spatially varying field inhomogeneities and energy-dissipating interactions between spins<sup>l</sup> change precessional rates, causing spin isochromats to become out of phase with each other. The dephasing is a time-dependent process, increasing linearly with time. The dephasing among individual spin isochromats ultimately leads to decreased aggregate transverse magnetization; therefore, the recoverable MR signal in the process known as *Free Induction Decay* (FID). The FID connotes the MR signal loss due to naturally occurring phenomena taking

<sup>k</sup> In the fast imaging applications, a smaller flip angle can be used, anywhere from  $\frac{\pi}{6}$  to  $\frac{\pi}{2}$ .

<sup>l</sup>  $T_2^*$  and  $T_2$  types relaxation, respectively.



place when the excited sample is left on its own after the excitation pulse and no additional external manipulations with spin isochromats are performed. The picture, however, changes when the gradient is turned on at the moment of time  $t = t_1$ .

Applying an extra gradient field along the  $z$  axis further intensifies the spin dephasing. Indeed, under the influence of the gradient field, the spin isochromats that experience stronger than usual field rapidly spring forward whereas those spins that sustain weaker than usual field are held back. Because of the general loss of phase coherence, the rapid decay of the magnetization continues until the gradient is turned off at the moment of  $t = t_2$ , when the aggregate transverse magnetization is essentially nonexistent. The beat pattern exhibited by the aggregate transverse magnetization is due to transient coherence improvements that occur when individual spin isochromats precessing at common multiple frequencies align in the transverse plane.

At the moment of time  $t_2$ , the gradient is turned off so that no additional gradient-induced coherence loss is incurred, and by the moment of time  $t_3$ , the South and North spin isochromats have reached their largest values of phase angles, respectively.

At the moment of time  $t_3$ , another gradient field of the same magnitude and direction, but opposite polarity, is applied to the sample. This gradient field forces previously fast-moving spin isochromats to slow down and assume precessional frequency of the spins that earlier were trailing during the dephasing portion. In a similar manner, the previously slow-moving spins are now chasing those that were moving faster during the dephasing segment. Assuming that the spin isochromats were forced to dephase from the state of full transverse coherence and ignoring the irrecoverable energy-dissipating losses due to interactions between spins<sup>m</sup>, the spin isochromats rephase and recreate the transverse coherence exactly after the period of time it took to dephase them, that is,  $\tau$ . The reinstated coherence is tantamount to a restored aggregate transverse magnetization, and thus newly formed echo; in this case, a gradient-echo.

It can be inferred that the amplitudes of the dephasing and rephasing lobes of the gradient may not be equal, such that the larger amplitude of the rephasing lobe expedites the coherence recovery. However, common to all gradient echo-like signal generation schemes is the combination of the dephasing and rephasing gradient lobes.

### Gradient-Echo Imaging Pulse Sequence

An implementation of a simplest—Fast Low Angle SHot (FLASH)<sup>n</sup>—gradient-echo pulse sequence is shown in Figure 2.7. The design of the gradient sequence includes such components common to all imaging pulse sequences such as the excitation structure, comprised of the RF excitation pulse and the slice selection gradient with the following

<sup>m</sup> As mentioned earlier, such losses are characterized by  $T_2$  relaxation time.

<sup>n</sup> Here and further in text the Siemens nomenclature is used.

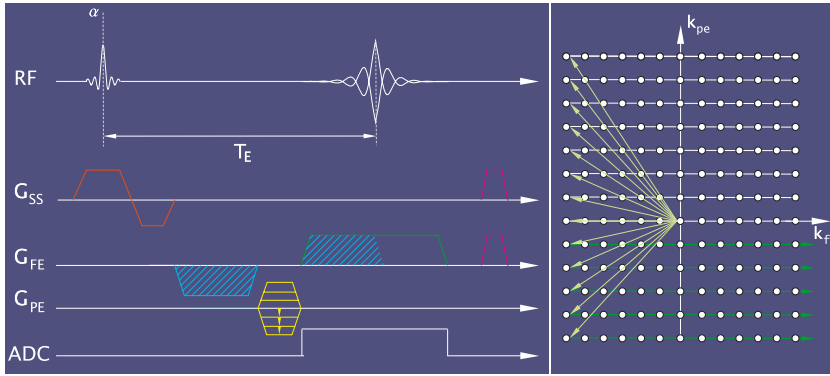


**Figure 2.7.** Gradient-Echo Timing Diagram.

rephasing lobe, and the data collection segment during which the echo is generated and associated MR signal is received. Moreover, it may include additional gradients called spoilers, which are employed to avoid a transverse steady state.

The spatial encoding in a conventional gradient-echo sequence is achieved in the same manner in which it is accomplished for the spin-echo counterpart. In particular, the spatial encoding in one of the directions is performed by conditioning spin isochromats' precessional frequency (the *frequency-encoding* direction), whereas the spatial information in the other direction is encoded by modulating the phase angle of spin isochromats (the *phase-encoding* direction). During the frequency-encoding period, the scanner's receiver circuitry is turned on and the MR signal returned by spin isochromats is recorded as the raw MR signal.

In the noticeable difference from the spin-echo implementation, the gradient-echo pulse sequence design does not retain a  $\pi$ -radian refocusing pulse. The lack of thereof is rather consequential. First, in the absence of the refocusing pulse, the RF power released by the coil and thus absorbed by tissues is reduced significantly. This factor makes sequences utilizing the gradient-echo signal recovery mechanism safer and more desirable in general. The reduced-energy deposition in the case of the gradient-echo sequence is especially salient when performed in higher field strength scanners (1.5 Tesla and up) because it requires larger amounts of RF energy to disturb a longitudinal equilibrium magnetization. Moreover, with the overall RF energy emission reduced, it is possible to pack more RF pulses closer together and therefore speed up the signal acquisition without a risk of exceeding Specific Absorption Rate (SAR) limits established by the U.S. Food and Drug Administration (FDA).

The absence of the refocusing pulse affects the sensitivity of gradient-echo sequences to magnetic field inhomogeneities and, consequently, the type of image contrast. The main effect of the refocusing pulse used in the spin-echo formation mechanism is achieved by nullifying phase angles of spin isochromats and reversing the direction of

the dephasing. Therefore, phase angles developed due to constant field inhomogeneities and magnetic susceptibilities are cancelled by the time of the echo.<sup>o</sup> Therefore, the spin-echo sequence has an inherent property to suppress MR signal contributions from large fixed inhomogeneities.

On the contrary, because it lacks the refocusing pulse, the gradient-echo sequence is very much sensitive to field inhomogeneities and magnetic susceptibilities. Indeed, instead of an RF refocusing pulse, the gradient-echo imaging pulse sequence employs a structure that contains alternating gradients to re-establish coherence of spin isochromats and generate the echo, as it is shown in the Figure 2.7. The overall phase change introduced by the gradients by the echo time is zero, as the phase change during the rephase segment is offset by the opposite phase change during the following dephasing segment. However, such a gradient reversal can only compensate for the spin phase gained or lost due to the gradient field itself. Any amount of spin phase advanced or retarded due to factors other than gradients fields, such as effects of sample-related magnetic susceptibilities, remain uncompensated at the echo time. In other words, phase angles, neither refocused nor compensated, continue to develop through the entire echo formation period, and thus are non-zero at the time of an echo, effectively reducing the MR signal.

Because the spin coherence is achieved by having reversal gradients to nullify spin phase changes, thus rendering the refocusing pulse unnecessary, the repetition time  $T_R$  now can be made shorter. Having been given less time to die down, the spin coherence at the end of the signal detection period turns out to be higher than that in the spin-echo case,<sup>p</sup> leaving a relatively stronger transverse magnetization to linger before the next excitation pulse.

In addition to the increased transverse coherence, the effects of consecutive RF pulses on the magnetization should be mentioned. It is known that a series of several arbitrary RF pulses is capable of producing spin echoes and so called stimulated echoes.<sup>16</sup> Generally, such echoes are not treated as a primary source of the gradient-echo MR signal, and thus are disregarded in the majority of gradient-echo pulse sequences. However, if allowed to propagate freely and undisturbed throughout subsequent repetition periods, the lingering magnetization responsible for the formation of such echoes may affect the gradient echoes formed later, and is likely to cause imaging artifacts. Moreover, coupled with the aforementioned enhanced transverse magnetization, the artifacts may have very consequential ramifications on the MR signal in pulse sequences where either transverse or longitudinal magnetization is maintained in the steady state.

There are two ways to mitigate the effects of unwanted MR signal echoes—to destroy the lingering transverse magnetization with addi-

---

<sup>o</sup> The field inhomogeneities and magnetic susceptibilities are assumed constant over the single  $T_R$ .

<sup>p</sup> It is due to the fact that less transverse magnetization is lost to irreversible  $T_2$  relaxation.

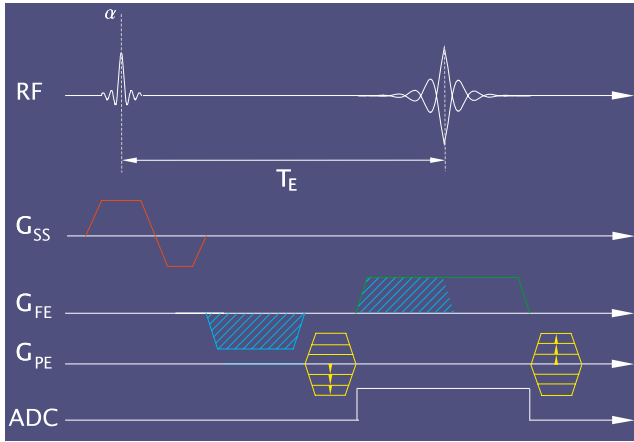


**Figure 2.8.** FISP Pulse Sequence Timing Diagram.

tional gradient fields or RF pulses, or to refocus magnetization components leading to formation of spin and stimulated echoes.

The methods of the first group use either additional gradients alone or coupled with quasi-random flip-angle RF pulses to further and irreversibly<sup>9</sup> dephase spins in the transverse plane, effectively destroying the remnant aggregate transverse magnetization. With the bulk transverse magnetization essentially nonexistent, only longitudinal component of the aggregate magnetization contributes to the fresh bulk transverse magnetization at the next RF pulse, which is during the next  $T_R$  period.

Alternative to the mechanism of spoiling of the bulk transverse magnetization is the process of refocusing its components, contributing to formation of spin and stimulated echoes. The first sequence to take advantage of the refocusing was fast imaging with steady precession (FISP).<sup>17</sup> In the most trivial way, it is achieved by adding an extra phase-encoding gradient to the existing FLASH-like pulse sequence, as shown in the Figure 2.8. Its function is to compensate for the phase change introduced by the initial phase-encoding gradient step. For that purpose, the new gradient has the same magnitude as the initial phase-encoding gradient field; however, it is applied in the opposite direction. The partial rephasing of the transverse magnetization allowed an additional  $T_2$ -weighted signal be recovered from refocused spin and stimulated echoes.

The reversal of gradients just in the direction of the phase encoding does not fully rephase transverse magnetization. Indeed, the phase of spin isochromats is changed by any disturbance, leading to the Larmor frequency variation, regardless of directionality of the such. In order to attain a fully refocused transverse magnetization and the largest

<sup>9</sup> So that the transverse magnetization created in this repetition period does not reform sometime later.

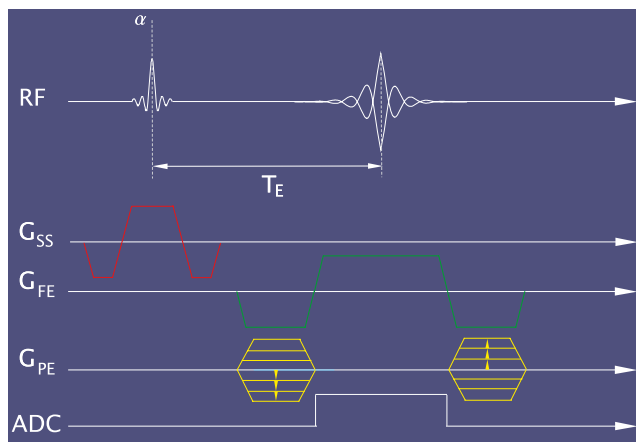


**Figure 2.9.** trueFISP Pulse Sequence Timing Diagram.

possible MR signal, the area under gradient lobes has to be zero in all three directions.

This approach is implemented in the pulse sequence known as true-FISP. The design of the trueFISP sequence (Figure 2.9) contains a train of equally spaced RF pulses and gradient structures balancing the phase in all three directions. Having the phase of the transverse magnetization at the end of the repetition period restored to its prepulse value improves overall transverse coherence, and thus the SNR while maintaining a relatively short  $T_R$  and higher receiver bandwidth. The recent studies showed that the trueFISP sequences are capable of recovering a relatively strong BOLD signal.<sup>18</sup>

## Contrast Characteristics of Gradient-Echo Sequences

### *Vascular Effects*

As in the case with the spin-echo pulse sequences, the diffusing motion of water molecules is a crucial and defining factor in the development of the gradient-echo contrast. The nature of diffusion effects is again due to microscopic phase variations that the water molecule experiences as it traverses through magnetic field gradients established by nearby vessels. However, although identical by nature, the diffusion effects are exhibited somewhat differently in case of the gradient-echo pulse sequences.

If the spatial extent of field variations created by larger venule vessels spans over distances larger than a diffusing molecule travels on average, it experiences a very similar field at any point of its trajectory. Without a refocusing pulse, the average phase displacement acquired by molecules due to these offset fields is increased linearly as a function of time and is not compensated at the end of the acquisition period. Consequently, due to the procured dephasing, the relaxation rate increases and the MR signal is weakened to a relatively higher degree.

When water molecules traverse several fields over their trajectory's average length, the phase offsets gained by water molecules are very similar; therefore, the range of phase offsets is minimal, as is the overall dephasing. The  $T_2$  relaxation rate, and thus the MR signal, remain largely unaffected. Such an attenuation regime is identical to that achieved with the spin-echo formation mechanism for vessels up to six micrometers in diameter.

The extent to which the MR signal is attenuated depends on the amount of the phase offset that spin isochromats accumulate during their traversal through field gradients over a specific time, usually the echo time  $T_E$ . Therefore, it can be inferred that the relaxation rate increases with the vessel's size.

It is noteworthy to compare the sensitivity of spin- and gradient-echo formation mechanisms to the BOLD-related changes as a function of vessel's size. It has been mentioned previously in this chapter that the spin-echo pulse sequences appears to be most sensitive to diffusion effects occurring in capillaries. In contrast, the sensitivity of the gradient-echo sequence reaches its maximum towards larger structures, like venules and small veins.

### *Inflow Effects*

The impact that the blood inflow has on the gradient-echo MR signal mechanism is quite different from that on the MR signal recovered in a spin-echo. In the case of the spin-echo sequence, contrary to the MR signal reduction caused by unexcited spins flowing into a region partially saturated after a series of closely following excitation pulses, the inflow of unsaturated spins leads to the increase of the MR signal collected by the gradient-echo sequence.

Consider an imaging slice with a vessel carrying flowing blood surrounded by stationary tissues. Continuous application of RF excitation pulses designed to nutate the longitudinal magnetization into the transverse plane by partial flip angles<sup>r</sup> may cause a condition called saturation. The spin ensemble within stationary tissues becomes saturated after a considerable number of RF pulses are transmitted in a rapid succession, each released before the longitudinal magnetization is allowed to recover fully to its equilibrium value,  $M_0$ . During the allotted time,  $T_R$ , only so much of the longitudinal magnetization gets restored so that at the end of current  $T_R$  period

$$M_z < M_0.$$

This implies that not all spins excited by the last excitation pulse have radiated RF photons and are returned to their stable state, and the next RF excitation pulse acts on the longitudinal magnetization  $M_z$ , which is restored only partially. Similarly, at the end of the next repetition interval, the longitudinal magnetization is not given to relax to its pre-pulse value,  $M_z$ , so that even less of the fresh longitudinal magnetization is available to be acted upon by the following excitation pulse.

---

<sup>r</sup> Partial is any flip angle which causes less than  $\frac{\pi}{2}$ -radian nutation.

Thus, each following RF pulse acts on smaller longitudinal magnetization than the previous one.

On the other hand, each RF pulse brings a magnitude of the longitudinal magnetization to the same value, since the RF pulse's flip angle is kept constant.<sup>s</sup> Because the magnitude of the pre-pulse longitudinal magnetization is falling and its post-pulse magnitude is maintained, it can be inferred that the reduction of the longitudinal magnetization gradually<sup>t</sup> ceases after a certain number of RF pulses. Such dynamics imply that the magnitude of the longitudinal magnetization becomes confined between its pre- and post-pulse values throughout the entire  $T_R$  interval. This happens when the number of excited spins returned to their stable state is equal to the number of spins excited by the following RF pulse.

Because few spins get excited by a new RF pulse and consequently return the signal at the end of the  $T_R$  interval, the pre-pulse magnitude of the longitudinal magnetization is only slightly different from its post-pulse value; thus, the amount of available MR signal from stationary tissues is reduced. On the other hand, fresh spins contained in the blood entering the imaging slice are not saturated at all because they did not experience all previous excitations. The spins from the flowing blood enter the imaging slice and become slightly saturated as they pass through it. Since less saturated spins are capable of returning higher MR signal than the more saturated, such a dynamic leads to an intense MR signal coming from the blood. The differences between sufficiently saturated stationary tissues and partially saturated moving blood can therefore be identified in the image contrast.

The degree of saturation sustained by the blood spins largely depends on the blood flow velocity, the  $T_R$  interval, and the amount of the RF energy transferred to the spins, which is tantamount to the flip angle. The increase of the MR signal occurs when the sufficient number of unsaturated spins enter the imaging slice over several  $T_R$  periods. In case of the relatively short  $T_R$  or a fast blood flow, the MR signal increases due to the partial desaturation by the fresh spins. However, with the longer  $T_R$  period, a larger number of the saturated spins may have sufficient time to return to the equilibrium so that the signal from stationary tissues increases and the contrast with the blood MR signal diminishes. In case of a relatively slower blood flow, for instance capillary flux, it may take a few more  $T_R$  intervals for entered spins to pass through the imaging slice. Experiencing more RF pulses, blood spin isochromats become more saturated, which also equalizes the contrast between MR signals from stationary tissues and blood.

In addition to their inflow sensitivity, the gradient-echo methods are likely—more so than those of a spin-echo variety—to produce an MR signal that reflects sample-induced magnetic susceptibilities and

<sup>s</sup> Of course, variable flip angles are possible,<sup>19</sup> however consideration of such is beyond of this chapter's scope.

<sup>t</sup> As a matter of fact, exponentially, with the exponent's power being negative.<sup>20,p127</sup>



scanner-related field inhomogeneities. Generally, the increased sensitivity of the gradient-echo methods to such perturbations originates from uncompensated spin phase contributions developed during an MR signal echo's formation.

Indeed, a spatially dependent field distribution gives rise to a corresponding spatially varying distribution of the Larmor frequency. In this case, even adjacent spin isochromats may happen to precess at slightly different frequencies, leading to the phase dispersion and loss of the aggregate transverse magnetization. As was pointed out in the previous section, it is due to the absence of a refocusing pulse that the phases acquired by spin isochromats due to sustained inhomogeneities other than gradient fields do not get cancelled, but rather continue to develop until the echo time. On top of a distribution of fixed Larmor frequency-affecting factors, there are various effects that further modulate local field: random motion of water molecules (diffusion), varying magnetic properties of blood and tissues (oxygenation/deoxygenation), and eddy currents.

Sample-induced susceptibilities alter local magnetic fields, thus causing inhomogeneities. The effects created by sample-related susceptibilities usually can be seen as signal enhancement/reduction near tissue–tissue and, even to a larger degree, tissue–air interfaces. Furthermore, image distortions may be observed in or near regions with cavities and sinuses, where the inhomogeneities are high.

Only in part does the severity of image distortions depend on the degree of the inhomogeneity. Equally consequential are the imaging parameters, such as receiver bandwidth, direction of phase encoding, image resolution, and others. The imaging parameters have to be changed with caution and with the understanding of the implications of such changes. For instance, raising the receiver bandwidth mitigates image distortions, especially so in the phase-encoding directions. However, it also would decrease the SNR.

## Echo Planar Imaging Methods

The generic gradient-echo sequence displayed in the Figure 2.7 acquires  $n$  MR signal samples sequentially, one by one, along a single chose  $k$ -space line per an excitation period. Therefore, it has to be repeated  $n$  times in order to create a  $n \times n$ -pixel image.<sup>u</sup> The acquisition time is reduced in the steady-state sequences, for their  $T_R$  values usually are shorter than that of a conventional FLASH-like gradient-echo methods. Although either of these sequences can be used to detect gross BOLD-related MR signal variations originated in areas that are capable of producing a relatively robust signal, such as visual or motor cortices, they are proved to be unfittingly sluggish to adequately resolve rather fine BOLD effects elicited by swift subtle cognitive and behavioral processes.

---

<sup>u</sup> A trivial case is considered here, as the  $n \times n$  pixel image also can be created from the undersampled MR signal pool using various reconstruction tricks.



The pulse sequence tailored for imaging of physiological markers of transient events and processes would acquire the MR signal needed to reconstruct the entire image in the shortest time possible, at the same time lasting sufficiently long enough for BOLD-inducing factors influencing the MR signal to develop. The demand for higher temporal resolution necessitates more rapid MR signal sampling. Certainly, the shortest acquisition time is attained when the entire  $k$ -space is covered after a single excitation pulse. The group of imaging methods that traverse the  $k$ -space in a single passing shot, or in a series of multiple shots or segments, make up a class of Echo Planar Imaging (EPI) techniques.

It is noteworthy to mention that although the EPI methods belong to the distinct class of imaging techniques, they are not based on nor do they establish entirely new acquisition principles. As a matter of fact, EPI pulse sequences use the same echo-formation mechanisms as spin- or gradient-echo methods, with an exception that they are very quick to traverse the entire  $k$ -space, and thus offer a drastic improvement in acquisition time.

### Echo Planar Imaging Pulse Sequences

As implied above, unlike the collection strategy employed in the conventional imaging that repeats excitation-sampling pair over every  $k$ -space line, a typical EPI pulse sequence collects and spatially encodes all MR signal samples necessary for a subsequent reconstruction of the entire image in a single acquisition period following an excitation pulse.

The schematics of a generic EPI pulse sequence is shown in Figure 2.10. Initially, a pair of gradients is applied in both the phase- and frequency-encoding directions in order to advance to the first sample point of the first  $k$ -space line. Then an oscillatory gradient is applied along the frequency-encoding direction so that the train of echoes is generated, each for every gradient lobe, positive or negative.

Such a waveform of the read-out gradient establishes alternating directions of traversing the read-out lines, whereas brief blip phase-encoding gradient pulses shift the current  $k$ -space location from one line to another in the phase-encoding direction. Such waveforms of the phase- and frequency-encoding gradients draw the zig-zag  $k$ -space trajectory shown in the right of Figure 2.10. As it can be seen on the  $k$ -space diagram, each line comes through the point of  $k_x = 0$ . This is the moment of time when the line-echo is formed. Each echo is produced in the same fashion as the gradient-echo, that is via an application of the bipolar dephasing–rephasing gradient structure. After every echo, the phase-encoding gradient advances the trajectory to the next line, and so on until the entire  $k$ -space is traversed.

It should be taken into account that although every gradient forms its own echo, only the echo that coincides with the  $k$ -space center, the so-called primary-echo where the net gradient encoding is zero, is taken to calculate the echo time. Because the effect of gradients on spins during the formation of this echo is minimal so that their precessional frequencies are very near the Larmor frequency established by the main

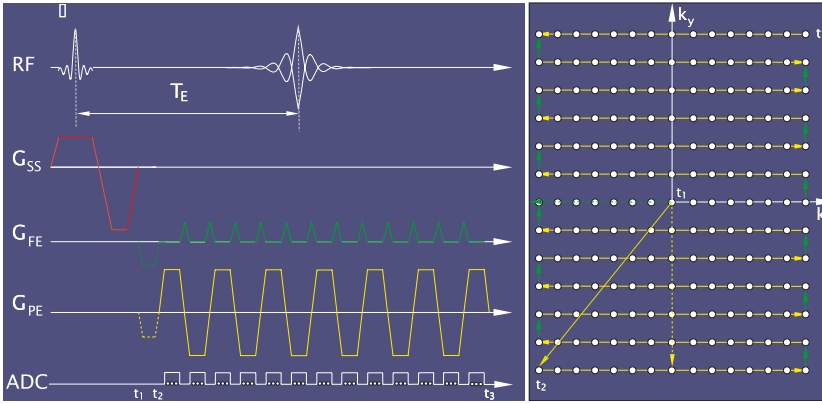


**Figure 2.10.** EPI Pulse Sequence Timing Diagram.

magnetic field  $B_0$ , the MR signal gain during this echo is the largest and determines the image contrast.

The implementation of the acquisition mechanism that allows a rapid collection of data to complete an entire image does not come without a few principle obstacles and challenges along the way. The accelerated sampling and shortened acquisition time that becomes comparable with such characteristic relaxation time  $T_2^*$  and  $T_2$  put additional demands on the scanner's gradient hardware, and the relaxation effects that influence the collected MR signal become more pronounced. In fact, the greatest challenge in the design of EPI sequences is imposed by the effect of the intrinsic decay owing to the  $T_2^*$  relaxation. Such an effect is twofold.

The  $T_2^*$  relaxation accounts for the global MR signal dropout across the entire image. Indeed, every  $k$ -space sample is attenuated by the signal decay during the acquisition, including the one located at the  $k$ -space center  $k_x = k_y = 0$ . Because this MR signal sample coincides with the primary and the strongest echo, the overall signal dropout is determined by the amount of the MR signal lost to the  $T_2^*$  relaxation at the time of passing through the  $k$ -space center. Thus, the effective  $T_E$  assigned to the time of the primary echo defines the overall loss of the MR signal.

Whereas the extent of the MR signal dropout depends on the position of the primary echo in respect to the  $T_2^*$ -relaxation decay profile, the length of the acquisition window determines the amount of the image blurring accounted to the  $T_2^*$  relaxation. Because the sampling through the entire  $k$ -space is performed within a single acquisition window, the MR signal may experience the  $T_2^*$  decay modulation large enough to cause a significant difference between the magnitude of MR signal samples acquired at the beginning and at the end of the acquisition window. In the zig-zag trajectory, it is high spatial frequencies ascribed by the peripheral  $k$ -space samples that get covered at the edges of the acquisition window. To this end, the substantial drop of the MR signal's amplitude over the acquisition window amounts to the image blurring.

Both caused by a decay due to the  $T_2^*$  relaxation, these effects are related, but somewhat separable. Consider an MR signal collected during a 20-millisecond long acquisition window with its primary echo located around  $T_E = 100$  milliseconds. If the shortest  $T_2^*$  is 40 milliseconds, only minimal blurring occurs because the amplitude of  $k$ -space samples acquired in the beginning of the window does not differ substantially from that acquired at the window's rear. On the other hand, the signal decays considerably by the time of the primary echo. Therefore, the image reflects the overall attenuation rather than the blurring effects. Alternatively, the blurring in the image made with the acquisition window of 100 milliseconds long and centered around  $T_E = 50$  milliseconds dominates over global attenuation effects.

Therefore, in order to mitigate the blurring, the length of the acquisition window has to be shortened. Usually, it is realized by increasing the reception bandwidth that allows faster MR signal sampling. The contrariety of the raised bandwidth is reduced image SNR. The length of the acquisition window also can be abridged by lowering the image resolution and thus the number of acquired  $k$ -space samples, for instance, from the image matrix of  $128 \times 128$  pixels to one comprised of  $64 \times 64$  pixels. In this case, in order to preserve the same coverage, the in-plane size of voxels is increased twofold. Having more spins in each voxel provides a larger per-voxel MR signal, and thus the SNR. However, it is more likely for a larger voxel to span intrinsic gradients caused by local inhomogeneities. To that end, the degree of the intravoxel inhomogeneity is also higher because it includes a wider range of frequencies; it inevitably shortens the  $T_2^*$  and decreases the SNR. The shorter  $T_2^*$  forces the  $T_E$  to decrease accordingly in order to maintain sufficient SNR, per global attenuation effect described above. On the other hand, the  $T_E$  has to be long enough to let the BOLD effect sufficiently modulate the MR signal.

Another aspect of the sampling process performed by an EPI pulse sequence is associated with characteristics of gradient coils. Implementation of EPI pulse sequences requires rather high gradient strength and switching rates in order to accomplish the rapid sampling. Based on the chosen field-of-view (FoV) and the resolution (image matrix), a size of the  $k$ -space grid that must be covered during the acquisition and the spacing between adjacent samples  $\Delta k$  are prescribed. From Equations (2.6–2.8), simplified for the case of a constant gradient, the distance between adjacent  $k$ -space samples is:

$$\Delta k = \gamma G \Delta t, \quad (2.13)$$

where  $\Delta t$  is the sampling rate. The FoV and  $\Delta k$  are directly connected as

$$\text{FoV} = \Delta k^{-1}. \quad (2.14)$$

The sampling rate can be found if the resolution  $N_{fe}$ ,  $N_{pe}$  and the duration of the acquisition window  $T$  are known:

$$\Delta t \approx \frac{T}{N_{fe} \cdot N_{pe}}. \quad (2.15)$$

In the most favorable case, when the duration of the excitation RF pulse<sup>v</sup> and the gap between its end and the beginning of the gradient waveform are neglected, the duration of the acquisition window is almost equal to the total acquisition time. The sampling rate can be readily found under such approximation conditions. If the pulse sequence is designed so that its primary echo occurs in the center of the acquisition window, then the total time is about twice the echo time,  $T = 2T_E$ . The estimated gradient amplitude can now be expressed through conventional imaging parameters:

$$G \approx \frac{N_{fe} \cdot N_{pe}}{2\gamma \cdot \text{FoV} \cdot T_E}. \quad (2.16)$$

Therefore, to acquire a 128-square-pixel image with the FoV of 220 millimeters and the echo time of 30 milliseconds, the highest gradient amplitude should be on the order of 30 milliTesla per meter (mT/m). Technically challenging to implement a mere five years ago, gradient fields of such magnitude are now considered typical, and they become increasingly available for research and clinical applications. Following recent FDA approval of operating MR scanners equipped with gradient coils capable of reaching gradient field magnitudes as high as 40 mT/m, such imaging techniques as EPI-based diffusion and perfusion and fMRI are now actively employed in clinical studies. Even higher gradient strengths, up to 1000 mT/m, are available on experimental human and animal scanners.

Another essential characteristic of gradient field hardware and coil is the slew rate that describes how fast the gradient field can be changed. It is defined as a ratio

$$\text{Slew rate} = \frac{\text{Gradient magnitude}}{\text{Rise time}},$$

where the rise time is the time required to advance the gradient amplitude from 0 to its maximum. Typical for clinical scanners, rise times may vary from 100 to 600 microseconds. The gradient ramping, the period of time during which the gradient's amplitude changes between its extrema is thus twice as long, if the rise time is constant. Therefore, the slew rate is on the order of few hundred Tesla per meter per second, with the most prevalent values being 100 to 200 T/m·s.

As the EPI pulse sequences are in essence a special way to traverse  $k$ -space and do not introduce fundamentally new echo formation principles, the same contrast mechanisms can be implemented using the EPI spatial encoding scheme.

### ***Gradient Echo-Recalled EPI Sequence***

The gradient echo-recalled EPI acquisition is the most commonly used imaging method in functional neuroimaging applications and research due to several reasons. First and foremost, although some amount of the  $T_2$  weighting is inevitably present because of the overall irreversible

---

<sup>v</sup> The duration of the excitation RF pulse ranges from two to five milliseconds.

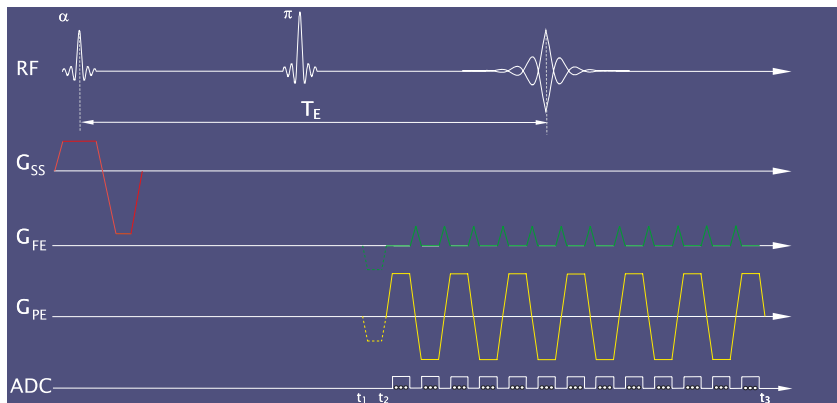


**Figure 2.11.** Spin-Echo EPI Pulse Sequence Timing Diagram.

transverse decay through the acquisition, the MR signal generated by this type of the EPI sequence carries a robust  $T_2^*$  contrast. The prevailing  $T_2^*$ -weighted contrast component comes from the sensitivity of the sequence's echo-formation mechanism to local field inhomogeneities. Because the nature of the BOLD contrast is exactly rooted in tiny field inhomogeneities imparted by variations in oxy/deoxyhemoglobin-induced blood susceptibility, the gradient-recalled EPI sequences are very appropriate for collection of BOLD-related MR signal changes sought in the functional imaging.

As in generic gradient-echo sequences, a smaller flip angle can be employed in gradient-recalled EPI designs without suffering large MR signal losses. The smaller flip angle makes it possible to decrease the  $T_R$  period, as less time is needed to restore the original longitudinal relaxation. Alternatively, a larger number of slices can be covered over the same  $T_R$  period. The optimal flip angle at which the gradient-echo-generated MR signal reaches its maximum, the Ernst angle, can be calculated to provide the best possible contrast.<sup>21</sup>

### *Spin-Echo Recalled EPI Sequence*

When the EPI spatial encoding mechanism itself is not a subject of interest but rather is taken as a component of a pulse sequence in whole, it can be considered as a black box that is designed to properly encode recovered MR signal and fill the  $k$ -space matrix. In case of a spin-echo pulse sequence, it is positioned following the excitation and refocusing RF pulses and all necessary gradient structures that define the image contrast, as is shown in the Figure 2.11.

The contrast-defining properties of the spin-echo-recalled EPI are similar to those of a regular spin-echo pulse sequence. In particular, although the spin-echo pulse sequence appears to be most susceptible to inhomogeneities imparted by capillaries, overall image contrast generated by this pulse sequence shows relatively little sensitivity to field inhomogeneities.

Somewhat more sensitive to BOLD-related changes in the  $T_2^*$  relaxation is the asymmetric spin-echo. As discussed earlier, a key feature

that differentiates it from the typical spin-echo pulse sequence is temporal misalignment between the center of the  $k$ -space (no spatial encoding condition) and the echo time. Such a mismatch usually is achieved by advancing the refocusing pulse and, consequently, the EPI spatial collection module towards the excitation pulse. In this case, there is a certain amount of  $T_2^*$  dephasing present at the moment of the contrast-defining central echo of the EPI read-out echo train, thus bringing about the imprint of BOLD-related inhomogeneities.

The benefit from using the ASE pulse sequence may become greater in higher field strengths, where the effects of constant inhomogeneities are amplified, and thus present an increasingly bothersome factor in SNR and overall image quality.

## Spiral-Echo Planar Imaging Methods

Because the EPI is just a clever trick to cover the entire  $k$ -space fast, there is no restriction on the trajectory along which the  $k$ -space is traversed. In fact, it can be quite arbitrary, as suggested by Dale and colleagues.<sup>22</sup> One of trajectories that has been proven effective to implement fast scanning technique while producing relatively high BOLD-related SNR resembles a spiral. Thus, the pulse sequence that utilizes such a trajectory is called spiral EPI pulse sequence. These sequences have been found effective in cardiovascular, renal,<sup>23,24</sup> and multiple functional brain imaging studies.<sup>25,26</sup> The imaging with spiral algorithms excels in these application because of its relatively low sensitivity to motion and flow and an efficient use of the gradient power.<sup>27</sup>

The term spiral refers to the method of the  $k$ -space traverse. In particular, the  $k$ -space trajectory is indeed a spiral, as shown in Figure 2.12. The spiral sequences do not constitute a whole new class of imaging

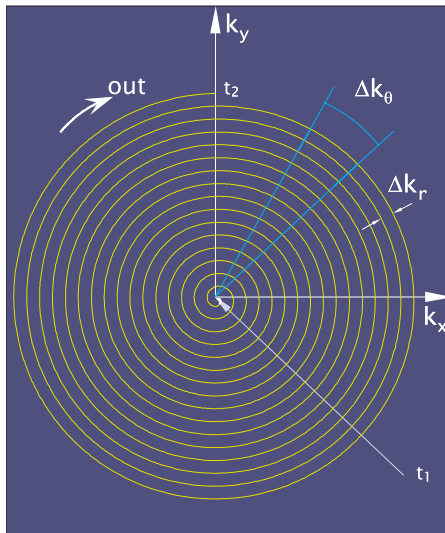


Figure 2.12.  $k$ -Space Diagram for Spiral EPI.

methods. Rather, they should be considered as a subset of EPI techniques because of many similarities between their designs, including collection of the MR signal corresponding to a large portion of the  $k$ -space with time-varying gradients following a single excitation pulse.

The design of a spiral pulse sequence involves two aspects. First, based on the mathematical expressions for a particular spiral trajectory and system-specific hardware characteristics, the gradient waveforms are calculated. The simplest type of the spiral trajectory, a so-called Archimedean spiral, is described by a running angle  $\theta$  as a function of the trajectory radius at a particular point along the spiral, as shown in the right portion of Figure 2.12:

$$k(t) = A\theta(t)e^{i\theta(t)}, \quad (2.17)$$

where the azimuthal angle  $\theta(t) = \omega_0 t$ , with  $\omega_0$  being a constant angular velocity. The gradient waveforms that implement the spiral traversal starting in the center and ending on the periphery of the  $k$ -space are shown on the pulse sequence diagram in Figure 2.13.

Other shapes of spiral trajectories are possible and widely used. For instance, in order to reduce physiologic noise effects that typically contaminate lower spatial frequencies, the vicinity of the  $k$ -space center often is oversampled by making more winds around the  $k$ -space's center, thus increasing the coverage density. To achieve an optimal density throughout the  $k$ -space and keep acquisition time from growing overly long, the varying sampling density spiral trajectory was proposed by Spielman and colleagues.<sup>28</sup> In this case, the image contrast improves because more MR signal samples are obtained around the center of the  $k$ -space and the contribution by physiological noise becomes limited.

Following the signal acquisition, a complementary image-reconstruction algorithm has to be applied to the raw signal data. The

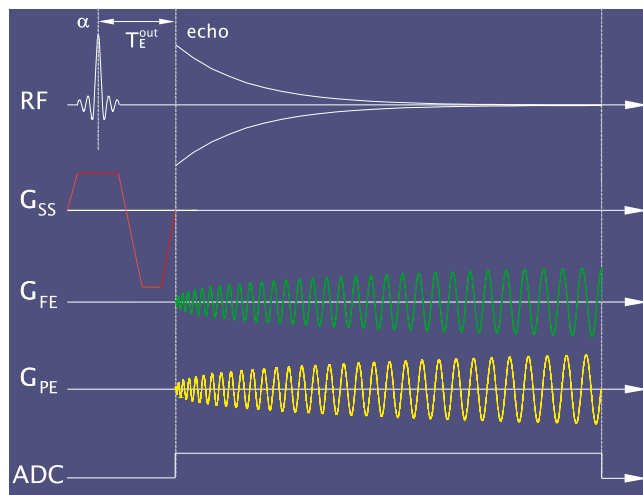


**Figure 2.13.** Spiral-Out Pulse Sequence Timing Diagram.



need for a gradient-specific reconstruction algorithm implementation is justified by limitations related to fast Fourier transformation (FFT) used to reconstruct the image from the raw MR signal. The regular FFT operation relies on a symmetrical and uniformly sampled rectilinear distribution of  $k$ -samples. This is not true for spiral-like traversals—not only do the collected data points not fall on the two-dimensional (2D) grid, but also their distribution is often nonuniform, as in case of the trajectory with the varying sampling density. Therefore, an operation that regrids the distribution of the  $k$ -samples into a rectilinear array and approximates the actual trajectory has to be applied before the data is submitted for the FFT.

There are seemingly two key ways to follow the spiral—namely, from the center to the periphery of the  $k$ -space and in the opposite direction. The spiral-out pulse sequence traverses the center of the  $k$ -space in the beginning of the acquisition period, and therefore obtains the contrast-defining echo immediately following the excitation pulse. In such a design, there is very little time to develop any appreciable  $T_2^*$  relaxation; the FID signal is strong and any motion did not have enough time to have an impact on the spatial encoding. On the contrary, the traverse in the opposite direction, from the periphery to the  $k$ -space center, leads to accumulation of  $T_2^*$ -related phase offsets that sensitizes the image contrast to the field inhomogeneities.

Each of these traversals has benefits and limitations that should be considered in the context of a specific application. In cardiac imaging, where motion and flow artifacts could be severe, the pulse sequence that is capable to limit contributions thereof to the MR signal is advantageous. Therefore, the spiral-out design is more desirable in cardiac and abdominal studies. On the other hand, in order to detect BOLD-related MR signal changes, the inhomogeneities have to be allowed to influence the MR signal. If the contrast-defining echo comes too soon after the excitation pulse, the phase offsets are negligible, thus limiting their effect on the MR signal. Therefore, in BOLD studies, the spiral-in pulse sequence is preferred.

There is, however a significant drawback associated with such a design. Namely, if the entire  $k$ -space is sampled over the single trajectory, the overall MR signal may experience a considerable  $T_2^*$  decay, leading to the decreased SNR. The solution to this particular predicament is to split the acquisition into several parts, covering the  $k$ -space in segments, so that the last echo appears earlier, but still at the end of the acquisition period. This approach reduces nonuniformity effects and eventually increases the SNR. However, the cardiac motion and respiration gives rise to undesirable image-to-image variations.

Several pulse sequence designs were proposed to accommodate the best of two traversals. For instance, one of designs is a two-segment acquisition that includes the spiral-in segment, followed by the spiral-out portion. In this case, both echoes, at the end of the spiral-in segment and at the beginning of the spiral-out portion, occur one after the other. Because the center of the  $k$ -space in each segment was acquired virtually at the same time, the two echoes have identical contrast. The MR signal collected during the leading spiral-in section is not severely



decayed, which reflects an inhomogeneity modulation. The MR signal recovered in the consecutive spiral-out segment does not experience any substantial inhomogeneity effects and does not suffer from ongoing  $T_2^*$  decay. Two  $k$ -space samples covered in both segments are later combined into a single  $k$ -space and the image is formed through the FFT. As expected, such an image can be sufficiently BOLD-modulated while sustaining sufficient MR signal magnitude and avoiding being degraded by  $T_2^*$  relaxation.

By default, the spiral sequences are GE, but they can be turned into SE, and also can be united to produce double-contrast sequences.

In summary, this chapter gives an overview of the various pulse sequences that currently are used today in fMRI BOLD imaging, as well as their characteristics. The appropriate choice of the pulse sequence and its optimal parameters are key factors in maximizing the BOLD signal for every fMRI experiment performed.

## References

1. Robitaille PM, Abduljali AM, Kangarlu A. Ultra high resolution imaging of the human head at 8 tesla:  $2K \times 2K$  for Y2K. *J Comput Assist Tomogr.* 2000; 24(1):2–8.
2. Guinnessy P. Powerful NMR mashines debut in USA. *Physics Today.* 2002;55(3):30–31.
3. Constans A. NMR hits the big time. *The Scientist.* 2003;17(7):45–47.
4. Clark DD, Sokoloff L. Basic neurochemistry. In: *Circulation and Energy Metabolism of the Brain*, New York: Raven; 1994:645–680.
5. Hasselbalch SG, Knudsen GM, Jakobsen J, Hagenman LP, Holm S, Paulason OB. Brain metabolism during short term starvation in humans. *J Cereb Blood Flow Metab.* 1994;14:125–131.
6. Schwartz WJ, Smith CB, Davidsen L, Savaki H, Sokoloff L, Mata M, Fink DJ, Gainer H. Metabolic mapping of functional activity in the hypothalamo-neurohypophysial system of the rat. *Science.* 1979;205:723–725.
7. Hyder F, Rothman DL, Mason GF, Rangarajan A, Shulman KL. Oxidative glucose metabolism in rat brain during single forepaw stimulation: A spatially localized  $^1H[^{13}C]$  nuclear magnetic resonance study]. *J Cereb Blood Flow Metab.* 1997;17:1040–1047.
8. Gross PM, Sposito NM, Pettersen SE, Panton DG, Fenstermacher JD. Topography of capillary density, glucose metabolism, and microvascular function within the rat inferior colliculus. *J Cereb Blood Flow Metab.* 1987;7:154–160.
9. Klein B, Kuschinsky W, Schrock H, Vetterlein F. Interdependency of local capillary density, blood flow, and metabolism in rat brains. *Am J Physiol.* 1986;251:H1333–H1340.
10. Fox PT, Raichle ME, Mintun MA, Dence C. Nonoxidative glucose consumption during focal physiologic neuronal activity. *Science.* 1988;241: 462–464.
11. Davis TL, Kwong KK, Weisskoff RM, Rosen BR. Calibrated functional MRI: Mapping the dynamics of oxidative metabolism. *Proc Nat Acad Sci USA.* 1998;95:1834–1839.
12. Thulborn KR, Waterton JC, Matthews PM, Padda GK. Oxygenation dependence of the transverse relaxation time of water protons in whole blood at high field. *Biochem Biophys Acta.* 1982;714:265–270.

13. Turner R, Le Bihan D, Moonen CT, Despres D, Frank D. Echo-planar time course MRI of cat brain oxygenation changes. *Magn Reson Med*. 1991;22: 159–166.
14. Feynman RP, Leighton RB, Sands M. *The Feynman Lectures on Physics*, vol. 1. Addison-Wesley Publishing Company; 1964.
15. Bandettini PA, Wong EC, Jesmanowicz A, Hinks RS, Hyde JS. Spin-echo and Gradient-echo EPI of human brain activation using BOLD contrast. A comparative study at 1.5T. *NMR Biomed*. 1994;7:12–20.
16. Hahn EL. Spin echoes. *Physical Rev*. 1950;80:580–594.
17. Oppelt A, Graumann R, Barfuss H. FISP: A new fast MRI sequence. *Electromedica*. 1986;54:15–18.
18. Scheffler K, Seifritz E, Bilecen D, Venkatesan R, Hennig J, Deimling M, Haacke EM. Detection of BOLD changes by means of a frequency-sensitive trueFISP technique: Preliminary results. *NMR Biomed*. 2001;14(7–8): 490–496.
19. Scheffler K, Hennig J. TIDE (transition into driven equilibrium)-sequences for brain imaging with improved signal and contrast behaviour. In: *Proceedings of ISMRM. 11<sup>th</sup> Scientific Meeting and Exhibition*. Toronto, Ontario, Canada: 2003:973.
20. Haacke EM, Brown RE, Thompson MR, Venkatesan R. *Magnetic Resonance Imaging: Physical Principles and Sequence Design*. New-York: John Wiley & Sons Inc.; 1999.
21. Ernst R, Anderson W. Application of Fourier transform spectroscopy to magnetic resonance. *Rev Sci Instrum*. 1966;37:93–102.
22. Dale B, Wendt M, Duerk JL. A rapid look-up table method for reconstructing MR images from arbitrary  $k$ -space trajectories. *IEEE Trans Med Imaging*. 2001;20(3):207–217.
23. Meyer C, Hu B, Nishimura DG, Macovshi A. Fast coronary artery imaging. *Magn Reson Imaging*. 1992;28:202–213.
24. Yacoe ME, Li KC, Cheung L, Meyer CH. Spiral spin-echo magnetic resonance imaging of the pelvis with spectrally and spatially selective radiofrequency excitation: Comparison with fat-saturated fast spin-echo imaging. *Can Assoc Radiol J*. 1996;48:247–251.
25. Noll DC, Cohen JD, Meyer CH, Schneider W. Spiral  $k$ -space MR imaging of cortical activation. *J Magn Reson Imaging*. 1995;5(1):49–56.
26. Cohen JD, Perlstein WM, Braver TS, Nystrom LE, Noll DC, Jonides J, Smith EE. Temporal dynamics of brain activation during a working memory task. *Nature*. 1997;386:604–608.
27. Nishimura DG, Irarrazabal P, Meyer CH. A velocity  $k$ -space analysis of flow effects in echo-planar and spiral imaging. *Magn Reson Med*. 1995;33: 549–556.
28. Spielman DM, Pauly JM, Meyer CH. Magnetic resonance fluoroscopy using spirals with variable sampling densities. *Magn Reson Med*. 1995;34:388–394.

Functional MRI

Basic Principles and Clinical Applications

Faro, S.H.; Mohamed, F.B. (Eds.)

2006, XIV, 534 p. 177 illus., 134 illus. in color.,

Hardcover

ISBN: 978-0-387-23046-7